Available online at www.sciencedirect.com
ScienceDirect
Journal of Computational Physics 218 (2006) 429–441
JOURNAL OF COMPUTATIONAL PHYSICS
www.elsevier.com/locate/jcp

Mesoscopic simulation of Ostwald ripening

David J. Horntrop *

Department of Mathematical Sciences, New Jersey Institute of Technology, Cullimore Hall – Mathematical Science, Newark, NJ 07102, United States

Received 25 July 2005; accepted 20 February 2006

Abstract

The self-organization of particles in a two phase system in the coexistence region through a diffusive mechanism is known as Ostwald ripening. This phenomenon is an example of a multiscale problem in that the microscopic level interaction of the particles can greatly impact the macroscale or observable morphology of the system. Ostwald ripening is studied here through the use of a mesoscopic model which is a stochastic partial integrodifferential equation that is derived from a spin exchange Ising model. This model is studied through the use of recently developed and benchmarked spectral schemes for the simulation of solutions to stochastic partial differential equations. The typical cluster size is observed to grow like $t^{\frac{1}{3}}$ over range of times with faster growth at later times. The results included here also demonstrate the effect of adjusting the interparticle interaction on the morphological evolution of the system at the macroscopic level.

MRC: 65C30; 68U20; 82C80

Keywords: Lifshitz–Slyozov growth law; Stochastic partial differential equations; Spectral methods; Mesoscopic models; Monte Carlo simulation

1. Introduction

Consider a two phase system in the coexistence region in which one component is less prevalent than the other. The coarsening phenomenon in which mass is transported via diffusion in such a two phase system is known as Ostwald ripening. In order to minimize the free energy of the system, the overall interfacial area of the system is reduced. In general, larger droplets of the minority phase grow at the expense of smaller droplets of the minority phase. The number of droplets decreases while the average size of the remaining droplets increases because of the conservation of mass in the system.

Ostwald ripening has proved to be quite difficult to study at least in part due to its inherently multiscale nature since molecular behavior greatly impacts the macroscale, observable behavior of such a system. One of the first successful theoretical results regarding Ostwald ripening was derived independently by Lifshitz

* Tel.: +1 973 596 5678; fax: +1 973 596 5591.
E-mail address: horntrop@njit.edu.

0021-9991/$ - see front matter © 2006 Elsevier Inc. All rights reserved.
doi:10.1016/j.jcp.2006.02.018

and Slyozov [1] and Wagner [2]. While most assumptions in [1,2] are the same, including the assumption of spherical particles which do not interact, Lifshitz and Slyozov assumed conservation of mass and Wagner assumed conservation of volume fraction. In spite of this difference, the conclusions are the same [3]. In the limit of zero volume fraction of the minority phase, it was asymptotically determined that the domain size of a typical cluster of particles should be a temporal power law. A simple scaling argument can be given which yields the LSW growth law [4] while more complete derivations of this growth law are given in the original papers [1,2] as well as the review articles [5–8]. The LSW growth law is

$$R \sim t^{\frac{1}{3}}, \tag{1}$$

where R denotes the size of a typical cluster and t is time.

While this result has been widely recognized as of great importance, the shortcomings of this theory due to the restrictive nature of its assumptions are also well understood. Particularly problematic is the assumption of no interparticle interactions. From the point of view of physical intuition, it seems reasonable that the coarsening of a domain depends upon the size and proximity of other clusters, e.g., an isolated cluster will behave quite differently than a cluster surrounded by other large clusters. The experimental results such as in [9] also demonstrate the importance of particle interactions during Ostwald ripening. Much modeling has been done in an attempt to incorporate these interactions in the framework of the LSW theory. The review articles in [6–8] describe and include references to this large body of work. One interesting recent mathematical result which also points out a difficulty with the basic LSW model appears in [3,10], where it was shown that the long time asymptotic behavior of solutions does not universally behave like a power law and is, in fact, strongly dependent upon the initial distribution of the particles.

Computation has played an important role in studies of Ostwald ripening. Boundary integral methods have traditionally been used in direct studies of the LSW model. See [11–14] for example and [15] for further references. Recently, a finite volume approach was used for a mathematically reformulated version of the LSW model in [16,17]. However, the greatest amount of computational work related to Ostwald ripening has been based upon the Cahn–Hilliard field theory model. While there has been some use of finite element methods for the Cahn–Hilliard equation [18–20], most computational work has focused on the use of finite differences. Because of the appearance of fourth derivatives in the Cahn–Hilliard equation, numerical stability restrictions on the choice of time step are quite severe; also, the choice of discretization must be made to preserve the conservation of mass in the system. In spite of these difficulties, many useful results have been obtained. For example, see [21–25].

In contrast to the macroscale models discussed above, microscale models which consider each individual particle in a system are also used to study Ostwald ripening. The most commonly used particle model which is appropriate for Ostwald ripening is the Ising spin exchange model. The simplest computational approach to this problem is to use Kawasaki's algorithm [26]; basically in this approach adjacent pairs of particles are selected at random and the determination of whether or not an exchange in value occurs depends on the Metropolis probability. Typical results from such simulations appear in [4,27,28]. Such an approach is very computationally intensive especially when the system has become fairly well-organized so that most adjacent pairs of particles have the same value thereby eliminating any possible effect of the exchange of that pair. Thus, a great deal computational resources are necessary to accomplish simulations for a long time with a large number of particles. Accordingly, many approximations and other speedups to Kawasaki's algorithm have been proposed; several are discussed in [4,28,29]. While a great deal of improvement in efficiency has been accomplished by these efforts, long time simulations are still difficult to obtain using such particle based methods, though recently developed coarse-grained Monte Carlo methods which are applicable to a wide class of problems in addition to Ostwald ripening show a great deal of promise in both accuracy and efficiency [30–32].

In this paper, recently derived mesoscopic models are used in a computational study of Ostwald ripening. These models are similar in spirit to the field theory models but arise directly from microscopic models. There are many attractive features of the mesoscopic model which alleviate many of the concerns with other models described in the previous paragraphs; in particular, mesoscopic models explicitly incorporate interparticle interactions. In the next section, these issues are discussed in much greater detail as part of the description of the mesosopic model for a conserved order parameter system. Section 3 describes the computational technique used in the simulation of the mesoscopic model. In Section 4, simulation results are given and compared

with the LSW growth law; the effect of changing the particle interaction length on the morphology and time scale of the coarsening process is also described. Finally, conclusions and areas for further study are given in Section 5.

2. Description of mesoscopic model

Mesoscopic models are local mean field theories that are designed to bridge the gap between microscopic (molecular) and macroscopic (observable) scales by directly incorporating microscopic level behavior in the macroscopic level. Details of the derivation of mesoscopic models are given in [33–37], though a brief qualitative description will be given in the following paragraph.

Mesoscopic models are derived through a coarse graining of the underlying microscopic system in a rigorous fashion without the introduction of artificial truncations. By calculating the average coverage over a ball with radius small compared with the interaction radius, the small random fluctuations will be averaged out while spatial variations in the coverage will still be captured since the radius of the ball is smaller than the interaction radius. In passing to the limit of infinite interaction radius, an evolution equation of the average coverage can be derived which includes stochastic terms. Such an approach can be followed for various micromechanisms while insuring that the underlying Gibbs measure remains invariant, i.e., detailed balance is satisfied.

There are many features of mesoscopic models which make them worthy of study. The ability to include stochastic noise terms in the mesoscopic model from a direct derivation rather than in an ad hoc manner is one of the particularly attractive features of this class of mesoscopic models. The fact that the mesoscopic model is a continuum model should allow for more efficient computer simulations as compared with the underlying particle model. In addition, the coupling of continuum models with other continuum models is much more straightforward than coupling of continuum models with particle models.

The mesoscopic model that would be an appropriate model of Ostwald ripening is derived from the spin exchange (surface diffusion) mechanism and is given by the following stochastic partial integrodifferential equation:

$$u_t - D\nabla \cdot [\nabla u - \beta u(1-u)\nabla J_m * u] + \gamma \mathrm{div}[\sqrt{2Du(1-u)}\mathrm{d}W(x,t)] = 0, \tag{2}$$

where u is the concentration of the minority phase, D is the diffusion constant, β is proportional to the inverse of the temperature of the underlying Ising model, J_m is the migration potential, γ is proportional to the interaction length of the particles, and $\mathrm{d}W$ represents a process that is delta correlated (white noise) in both space and time with

$$\langle \mathrm{d}W(x,t) \rangle = 0$$

and

$$\langle \mathrm{d}W(x,t)\mathrm{d}W(x',t') \rangle = \delta(x-x')\delta(t-t'),$$

where the angular brackets are used to denote mean values. It is important to observe that the noise in (2) is multiplicative rather the additive noise that is commonly added to deterministic models in an ad hoc manner. It is also noteworthy that the Cahn–Hilliard equation can be obtained from (2) by a suitable rescaling and Taylor expansion and thus is a special case of (2) [37].

The model in (2) has many features which make it attractive for studying Ostwald ripening. Especially useful is the explicit appearance of the interaction potential which transparently and directly allows for the consideration of a wide variety of interparticle interactions, unlike the LSW theory and its variants. The stochasticity of this models has both virtues and drawbacks. The randomness should reduce the likelihood of there being sensitive dependence on the initial data; however, the randomness necessitates averaging over several realizations in computational work.

A computational study of the mesoscopic model in (2) is described in this paper. Numerical techniques for stochastic partial differential equations such as (2) have received limited attention in the literature. Finite difference methods appear in [38–44]. Stochastic finite elements are discussed in [45] and applied to stochastic partial differential equations driven by white noise in [46–48]. While these numerical methods could be used

to simulate (2), the focus here is on spectral methods. While spectral methods have been used previously for stochastic partial differential equations with additive noise [49], their application for equations with multiplicative noise is novel [50]. There are a number of reasons why a spectral method seems to be a particularly attractive computational approach for (2). Certainly the calculation of convolutions is straightforward and efficient in a spectral method. In [37], it was demonstrated for a deterministic mesoscopic model that spectral methods were more accurate than finite difference methods for a comparable computational effort. When time stepping is done in Fourier space, spectral methods also allow for terms which become linear in Fourier space, such as diffusive terms, to be treated exactly using an integrating factor, thereby both increasing accuracy and directly reducing computational time. The integrating factor also eases stability restrictions on admissible time steps thus allowing the use of larger times steps than are numerically stable if the linear terms were not calculated exactly [51].

A large deviation principle argument has been given which shows that the probability that (2) differs from the underlying particle system decays exponentially [52,53]. One of the main goals of this paper is to provide computational evidence of the validity of the mesoscopic model in (2) in addition to the above analytic evidence. Another goal is to show that mesoscopic modeling and simulation is a practical means through which to study Ostwald ripening. Finally, a goal is to demonstrate the importance of the interparticle interactions on Ostwald ripening and the influence these interactions can have on the observable morphology of a system.

3. Description of simulation method

The numerical scheme that is used to study the mesoscopic model in (2) is based upon a generalization of spectral schemes for deterministic partial differential equations to the stochastic setting. For the sake of simplicity in the description of the spectral method in this section, it will be assumed that the stochastic partial differential equation in (2) has only one spatial dimension. This method straightforwardly generalizes to higher spatial dimension as evidenced by the two spatial dimension results presented in Section 4 of this paper.

Spectral schemes for deterministic evolution equations form the starting point for the development of spectral techniques for the simulation of solutions to (2). The solution of the equation is expanded in a Fourier series in the spatial component

$$u(x,t) = \sum_{\xi} \hat{u}(\xi,t) \mathrm{e}^{2\pi \mathrm{i} \xi x}. \tag{3}$$

Derivatives are treated in Fourier space where they are multiplies and a fast Fourier transform (FFT) is used to pass between physical space and Fourier space as needed. The resulting system of ordinary differential equations is solved using a finite difference time stepper; typically this system of ordinary differential equations is solved in Fourier space to take advantage of the existence of integrating factors to treat terms which are linear in Fourier space exactly.

A detailed description of the generalization of this approach to stochastic partial differential equations such as (2) is given in [50]. The emphasis of the discussion in the remainder of this section will be on those aspects of the scheme which are unique to the stochastic system, such as the spectral treatment of the multiplicative noise term in (2) and the use of a suitable time discretization technique.

3.1. Treatment of noise term

One of the most important steps for developing a spectral scheme for a stochastic partial differential equation such as (2) is to obtain a spectral representation for the spatial component of the noise term. It is well-known in the stochastic processes literature [54] that a stationary, isotropic, Gaussian random field $v(x)$ can be represented by the following stochastic integral in Fourier space:

$$v(x) = \int \mathrm{e}^{2\pi \mathrm{i} x \cdot \xi} S^{\frac{1}{2}}(\xi) \mathrm{d}W(\xi), \tag{4}$$

where W is Brownian motion and S is the spectral density function of the random field v. Most consistent numerical schemes for the simulation of random fields are based upon discretizations of this stochastic integral

[55–61]. The simplest such discretization uses equispaced nodes and is known as the Fourier method since this discretization results in what is essentially a Fourier series. This approximation can be written as

$$v(x) \approx \sum_{j=1}^{M} a_j \cos(2\pi\xi_j x) + b_j \sin(2\pi\xi_j x), \tag{5}$$

where a_j and b_j are independent Gaussians with mean zero and variance $S(\xi_j)\Delta\xi$. Due to the periodicity of the approximation in (5), the Fourier method is not suitable in applications in which the desired random field has long range correlations [55–58]. However, since the random field that is needed for the numerical study of (2) has delta correlation (lacks long range correlations), the Fourier method should provide a good approximation. The Fourier method is also computationally attractive since an FFT can be used directly to evaluate (5) at all physical space lattice sites.

The next issue in the treatment of the noise term in (2) is determining how to use (5) to obtain a spectral representation of the multiplicative noise term. Because each realization of the noise at a given time is approximated by a Fourier series representation (5), the noise term in (2) can be calculated by completing all multiplications in physical space and all differentiations in Fourier space, passing back and forth between physical space and Fourier space as necessary using an FFT. Thus, the existence of the Fourier series representation of the noise allows the treatment of the stochastic term in the same basic fashion as in spectral methods for deterministic partial differential equations.

3.2. Time discretization

Now that the spatial components have been computationally treated, the solution of the stochastic partial differential equation in (2) effectively has been reduced to the solution of a system of stochastic ordinary differential equations, any one of which can be written in the form

$$u_t = a(u)\mathrm{d}t + b(u)\mathrm{d}W(t), \tag{6}$$

where a is the drift coefficient and b is the diffusion coefficient to use the standard nomenclature from the stochastic ordinary differential equations literature [62]. Note that it is not appropriate to directly apply schemes that were derived for deterministic ordinary differential equations to (6) since the additional stochastic corrections from the Ito calculus must be included. As an example, it has been shown in [62] that the Euler method applied to a stochastic ordinary differential equation has a strong (pathwise) order of convergence of $\frac{1}{2}$ rather than order 1 as in the deterministic setting. Thus, it is essential to use schemes that are derived directly from suitable truncations of Taylor–Ito series rather than deterministic Taylor series. However, such properly derived schemes typically include derivatives of the drift and the diffusion coefficients. Given the highly non-linear nature of these terms in (2) and the fact that time steps will be taken in spatial Fourier space, it is especially useful to consider derivative-free Runge–Kutta type schemes [62–64]. One choice of a first-order strong scheme is the following:

$$u_{n+1} = u_n + a(u_n)\Delta t + b(u_n)\Delta W_n + \frac{1}{2\sqrt{\Delta t}}[b(\tilde{u}_n) - b(u_n)][(\Delta W_n)^2 - \Delta t], \tag{7}$$

with supporting value $\tilde{u}_n$ given by

$$\tilde{u}_n = u_n + b(u_n)\sqrt{\Delta t}, \tag{8}$$

where ΔW_n is a Gaussian with mean 0 and variance Δt. Of course, since the solution of (2) is real, the ΔW_n's in the time stepping scheme (when taking time steps in Fourier space) must be selected to respect the symmetries in Fourier coefficients that are present in spectral representations of real fields, i.e., $\bar{\hat{u}}(\xi, t) = \hat{u}(-\xi, t)$ where the overline denotes complex conjugate.

In [50], a wide variety of stochastic partial differential equations for which it is possible to analytically obtain the equilibrium covariance are used as computational benchmarks for the scheme described above. Included among these exactly solvable benchmarks is an equation with a noise term which has exactly the same form as the noise term in (2). Good agreement between simulation results and analytic results was obtained for a wide variety of choices of spectral density function S that would be appropriate to approximate

white noise. In fact, the most straightforward choice of $S(\xi) = 1$ was so successful in practice on those model problems that this choice was used to obtain the results presented in Section 4. All the results in [50] were shown for 5000 realizations in order to insure the sampling error was negligible so that the focus of that work could be on other accuracy issues surrounding the spectral method; however, results having errors typically less than 3% were obtained when only 500–1000 realizations were used, thus indicating that such quantities of realizations are sufficient in practice.

4. Simulation results

In this section, simulation results for (2) in two space dimensions using the numerical scheme described in Section 3 are given and described. The migration potential is chosen to be

$$J_m(x) = \frac{1}{\sqrt{\pi r_0^2}} \exp\left(\frac{-|x|^2}{r_0^2}\right), \tag{9}$$

with r_0 a parameter that describes the interaction length. Thus, shorter range interactions are stronger than longer range interactions and the interactions are isotropic in nature. The other parameters in (2) are chosen to be $D = 0.1$, $\beta = 6$ and $\gamma = r_0^2$. Simulation parameters include 64 wave numbers in each direction and a step size of $\Delta t = 0.00001$, which insures numerical stability of the time evolved in (7) and (8). The computational domain is a unit square with periodic boundary conditions. The system is initialized such that $\langle u(x,0)\rangle = 0.25$ with small amplitude perturbations about this mean. The time evolution of the mean can be used as a diagnostic of the simulations; it was observed to be virtually constant in all of the simulations presented below, as expected for this conservative system. Under these parameter choices and initialization, it would be expected that in the beginning several small regions of high and low concentration would form. In order to minimize the free energy, the system will evolve in such a way as to minimize the curvature of the regions of high concentration. Thus, the number of these regions will decrease, while the average size of them will increase. Eventually, there should be only one region which will become circular in its final state.

Fig. 1 contains contour plots of a typical concentration field obtained via simulation of (2) using the spectral scheme described in Section 3 for the case $r_0 = 0.05$ for times 1, 2, 3, 4, 5, 6, 8 and 10. The light areas represent regions of high concentration while the dark areas represent regions of low concentration. Each contour line represents a change in concentration of 8% relative to the mean concentration; the contours are centered about the mean concentration. All deviations in concentration field that are more than 44% from the mean value are not distinguished in these contour plots. The self-organization is readily apparent at even the earliest times depicted in Fig. 1; at intermediate times, an almost stripe-like structure can be observed; at later times, the system evolves to two circular regions. In later time results not shown here, the smaller circle disappears leaving one large circle by time 15. The total concentration in the system was observed to be conserved for all times considered, including this final state. All of these results are in qualitative agreement with those expected based on physical reasoning; while these simulations contain longer time results than those reported in the previously referenced studies of others using different mathematical models and numerical techniques, there is still good qualitative agreement over those times in common.

In order to quantify the simulation results and make comparisons with the LSW growth law in (1), it is necessary to have a way to measure the typical length scale in the concentration field. An approach commonly taken in the literature (e.g. [21,23,65]) in studies of the Cahn–Hilliard equation is now described. This approach is based upon statistical quantities such as the covariance and spectral density function of the concentration. (Note that the spectral density function has been referred to as the structure function in those references.) For a single realization of the concentration field, the covariance of the concentration is defined as the following spatial average over the lattice sites

$$B(x,t) = \frac{1}{N^2}\sum_{x'} u(x'+x,t)u(x',t) - \langle u\rangle^2, \tag{10}$$

where $\langle u\rangle$ is the mean of the concentration field which is a constant for (2) due to conservation. Under the assumption of isotropy, B depends only on the radial distance and can be obtained by averaging over spherical shells.

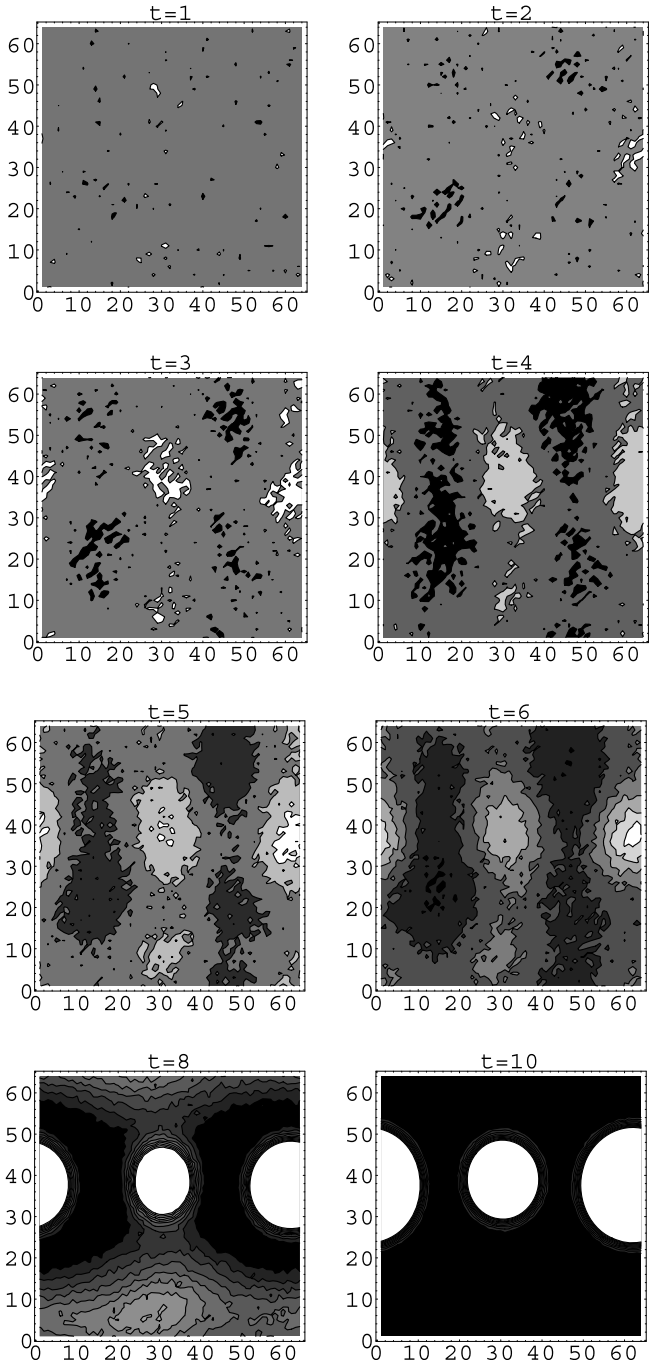

Fig. 1. Contour plots showing the time evolution of the concentration field obtained from mesoscopic simulations of (2) for the choice of interaction parameter $r_0 = 0.05$. The lighter shades represent regions of higher concentration while the darker shades represent regions of lower concentration. The expected self-organization into regions of high concentration is observed. By time 15 (not shown), the system has organized into a single circular region of high concentration.

The typical length scale of the concentration field can be determined by looking at the Fourier transform of the covariance field which is the spectral density function

$$S(\xi, t) = \widehat{B}(x, t). \tag{11}$$

If the covariance itself has not already been reduced to one dimension by spherical averaging, the resulting spectral density function is averaged over spherical shells to yield a one dimensional spectrum. The value of the wave number at which the spectrum has its maximum value would then correspond to the typical length of the concentration field. However, the numerical determination of this number can be quite difficult; thus, the first moment or mean of the spectral density function can be used as a measure of the typical length scale of the system. For a discrete system, the first moment can be written

$$\xi_1(t) = \frac{\sum_\xi \xi S(\xi, t)}{\sum_\xi S(\xi, t)}, \tag{12}$$

when the sum in the denominator serves to normalize the spectral density function. The typical length scale of the system is thus

$$R \sim \frac{1}{\xi_1(t)}. \tag{13}$$

The lack of radial symmetries in the concentration field at the later times depicted in Fig. 1 indicate this approach to measuring typical domain size will only be appropriate at earlier times in these simulations. Also at later times when the system consists of a low (below the mean value) concentration background with circular regions of high concentration, the regions of low concentration will significantly contribute to the covariance of the concentration field thus diminishing the effectiveness of this quantity as a measure of the size of the high concentration regions.

Thus, due to these considerations, Fig. 2 contains a log–log plot of the typical length scale as defined in (13) versus time only up to a value of 3. Averaging was done over 500 independent realizations of solutions to (2). The dots represent the average of the simulated values while the solid line on the plot is a visual reference for the $t^{\frac{1}{3}}$ growth law. A simple sampling calculation indicates that the standard deviation of these results is less than 2% of the value at all times presented in Fig. 2; thus, error bars are not included in the plot for the sake of visual clarity. There is a very clear interval of time over which the typical domain is growing according to this law which is roughly indicated by the solid line in Fig. 2; a least squares fit over that interval gives a power law exponent of 0.35 ± 0.02. At later times, the system is observed to transition to even faster growth with a power law exponent of 0.55 ± 0.03. While simulations at much lower volume fraction of the minority component have shown transitions in the growth law prefactor [66] which are supported by screening length arguments [67–69], the transition observed here is very different in that it occurs in the exponent of the power law rather than in the prefactor.

One of the important features of the mesoscopic model in (2) is the ease with which the interparticle interaction potential can be changed. The effect of adjusting the interaction length r_0 in the interaction potential in (9) is demonstrated in Figs. 3 and 4. Fig. 3 contains simulation results for $r_0 = 0.04$ at times 1, 2, 3, 4, 5 and 10. All other simulation parameters are unchanged from those used to obtain Fig. 1; the initial concentration field

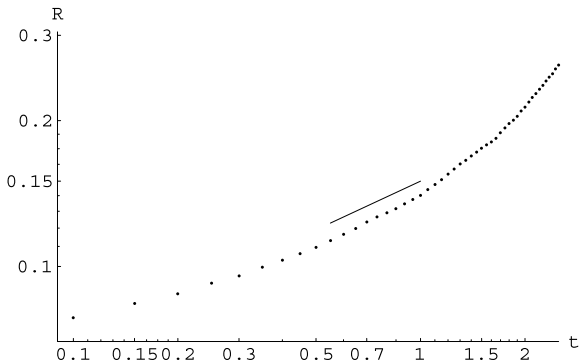

Fig. 2. Log–log plots showing the typical length scale of the self-organizing system calculated using (13) versus time. The solid line is $t^{\frac{1}{3}}$ and is given for the sake of visual comparison. The simulations clearly exhibit an interval of growth with a power law exponent very close to the $\frac{1}{3}$ of the LSW theory. At later times, the growth is observed to be a power law with exponent a bit larger than $\frac{1}{2}$.

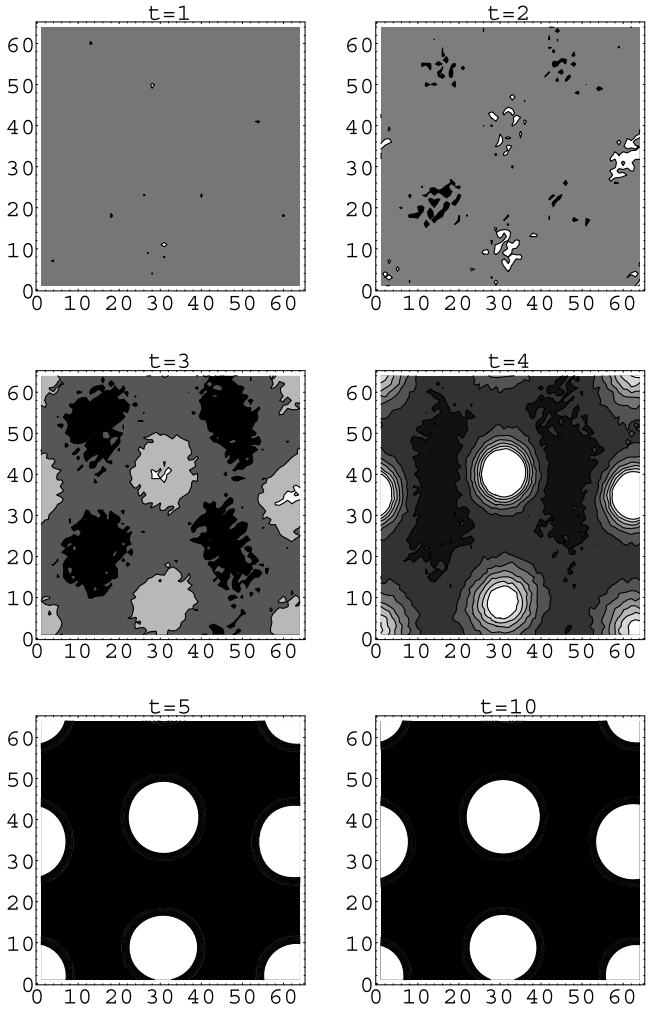

Fig. 3. Contour plots showing the time evolution of the concentration field obtained from mesoscopic simulations of (2) for the choice of interaction parameter $r_0 = 0.04$ which is smaller than that of Fig. 1. The contours and shading are the same as in Fig. 1. The organization into several circular regions occurs much more rapidly than in Fig. 1; however, the system does not evolve into a single circular region of high concentration until after time 40 (not shown).

is also unchanged; the contours for this figure were also obtained in the same fashion as those for Fig. 1. There are many striking qualitative differences in the concentration field in Fig. 3 with smaller interaction length than in Fig. 1. At the earlier stages, the self-organization into regions of high concentration surrounded by areas of low concentration occurs much more rapidly. It is especially noteworthy that more circular regions of high concentration but with smaller diameter formed in this case; there were four circles for $r_0 = 0.04$ but only two for $r_0 = 0.05$. However, a much greater amount of time was required for this configuration to evolve to its final state which is a single circular region of high concentration. The final configuration was not reached until after time 40 for $r_0 = 0.04$ versus by time 15 for $r_0 = 0.05$. Thus, while the initial organization was faster, the final stages of the evolution were much slower for the smaller value of r_0.

Results for $r_0 = 0.06$ are given in Fig. 4, where the increased value of r_0 is the only change when compared with Figs. 1 and 3. Fig. 4 contains contour plots at times 1, 2, 3, 4, 6, 8, 10 and 12. Particularly noteworthy is how much more slowly the system with larger interaction length initially evolves in order to reach a state with circular regions of high concentration in a region of overall low concentration. Moreover, this configuration consisted of two circles with one substantially larger than the other rather than the two circles that were closer in size for $r_0 = 0.05$. In spite of the relative slowness to reach this state, the final configuration was reached just

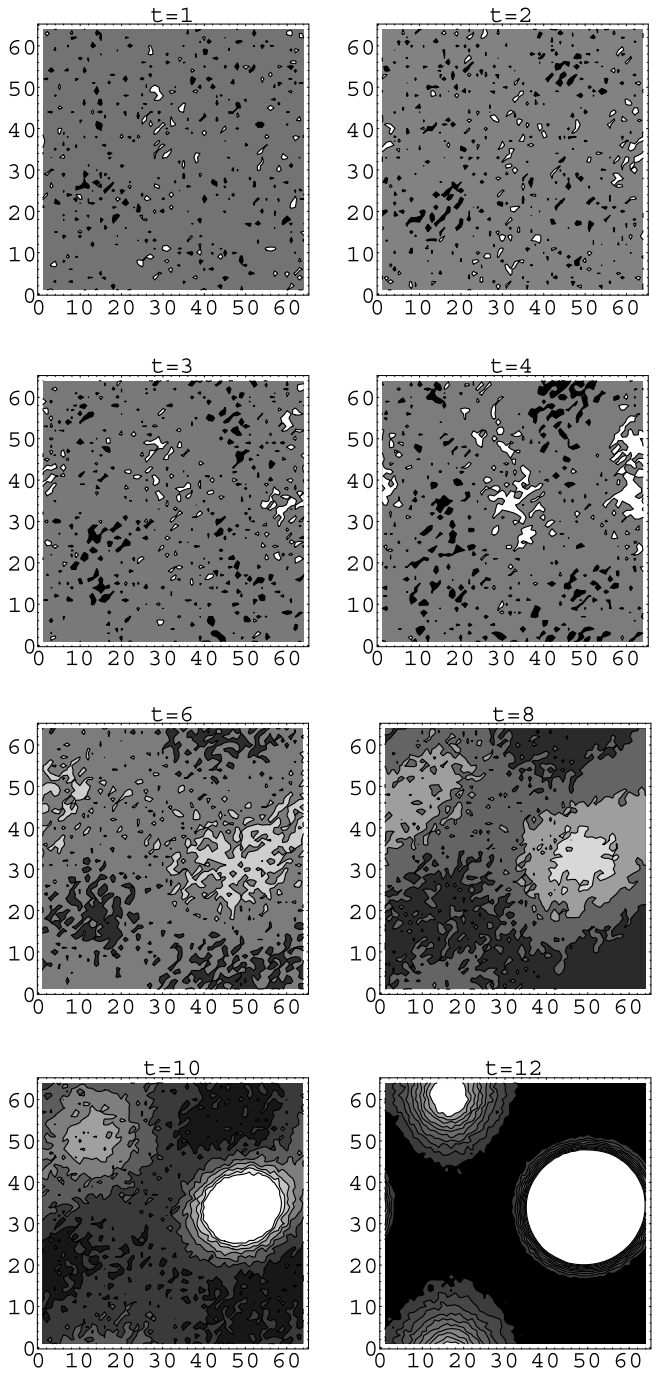

Fig. 4. Contour plots showing the time evolution of the concentration field obtained from mesoscopic simulations of (2) for the choice of interaction parameter $r_0 = 0.06$ which is larger than that of Figs. 1 and 3. The contours and shading are unchanged from Figs. 1 and 3. Slower initial self-organization into circular regions is observed; however, the final state of a single circular region of high concentration is reached more rapidly in this case (by time 13).

after time 13 for $r_0 = 0.06$ versus by time 15 for $r_0 = 0.05$. Thus, the larger interaction length tends to slow the initial self-organization yet accelerate the evolution from the intermediate state to the final state. Shorter interaction lengths allow for smaller structures to form at intermediate states.

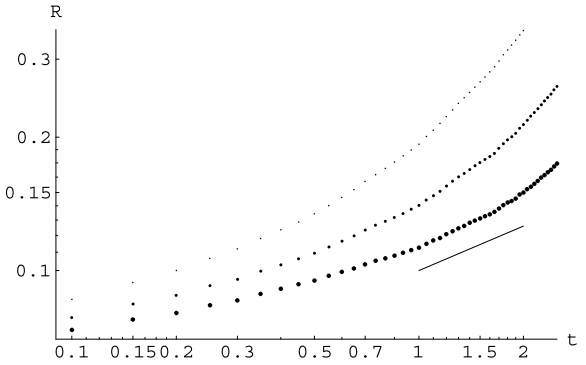

Fig. 5. Log–log plots showing the typical length scale calculated using (13) versus time for $r_0 = 0.04$ (small dots), 0.05 (medium dots) and 0.06 (large dots). The solid line is $t^{\frac{1}{3}}$ and is given for the sake of visual comparison. All cases have an interval of growth with a power law exponent very close to the $\frac{1}{3}$ of the LSW theory. As expected from Figs. 1, 3 and 4, self-organization occurred more rapidly for smaller values of r_0 at these times.

Fig. 5 is a comparsion of the typical length scale calculated using (13). The smallest dots correspond to $r_0 = 0.04$; the medium dots are for $r_0 = 0.05$; the largest dots represent $r_0 = 0.06$. The solid line is a $t^{\frac{1}{3}}$ power law which is given for the sake of visual comparison. Just as for Fig. 2, the standard deviation of the values at all times presented is less than 2%. For all cases, there is a region of growth close to $t^{\frac{1}{3}}$ before later regions of more rapid growth. For example, a least square fit of a power law function when $r_0 = 0.06$ calculated over the time interval indicated in the plot yielded an exponent of 0.37 ± 0.03 which is very close to the value of $\frac{1}{3}$ predicted by the LSW theory. In all cases, regions of growth with the same exponent occur for roughly the same values of the typical length size, e.g., intervals were the growth behaves like $t^{\frac{1}{3}}$ occur when the typical domain size is near 0.11. Also of note in this plot is the fact that the smaller values of the interaction length r_0 led to the faster self-organization at earlier times, just as had been observed in the contour plots in Figs. 1, 3 and 4.

5. Summary

This paper has demonstrated the value of the mesoscopic modeling approach used in conjunction with a spectral simulation scheme for stochastic partial differential equations. In addition to results that would be expected for self-organizing systems, other interesting and new results were obtained. The LSW growth law was observed to hold over some intermediate time intervals as self-organization proceeds from an initially disordered state in the simulations presented here. Given that the spectral computational scheme was numerically benchmarked in [50], these results provide computational evidence of the validity of the mesoscopic model in (2) in addition to the already existing large deviation principle arguments [52,53]. At later times, the self-organization was observed to continue to proceed according to a power law but with a larger exponent than predicted by the LSW theory.

Many other features of the mesoscopic simulation approach have also been demonstrated in this paper. The results given here indicate the practicality of mesoscopic simulation as a means of studying the long time behavior in a self-organizing system, certainly for much long times and larger systems than can be studied with molecular dynamics approaches. The ease with which interparticle interactions can be changed in mesoscopic simulation and the importance of the interparticle interactions on the morphology and time scale of the evolution was also demonstrated. Systems with shorter interaction lengths tended to more rapidly organize into intermediate states of smaller size when compared with systems with longer range interactions. However, evolution to the final state that consists of a single circular region of high concentration from the intermediate state that consists of multiple such circular regions proceeds much more rapidly for the larger interaction lengths.

Clearly further studies of the longer time behavior of the self-organizing system are warranted. Alternative means of characterizing the typical domain size will be needed for such studies given the limited range of applicability of the standard technique used in this study. One approach that will prove to be useful is the study of

self-organization in system with special geometric configurations. For some results of this sort, see [70]. Given the ease in which different sorts of particle interactions can be used in mesoscopic models, there are many additional classes of interaction potentials which should be considered. Potentials with repulsive interaction ranges would be encountered in systems with charged particles. Anisotropic potentials would naturally arise in coarsening systems in which there is a preferred growth direction.

Acknowledgments

The author thank Markos Katsoulakis for many useful conversations. This research is partly supported by NSF-DMS-0219211, NSF-DMS-0406633 and an NJIT SBR Grant.

References

[1] I. Lifshitz, V. Slyozov, The kinetics of precipitation from supersaturated solid solutions, J. Phys. Chem. Solids 19 (1961) 35–50.
[2] C. Wagner, Theorie der alterung von niederschlägen durch unlösen, Z. Elektrochem. 65 (1961) 581–594.
[3] B. Niethammer, R. Pego, The LSW model for domain coarsening: asymptotic behavior for conserved total mass, J. Stat. Phys. 104 (2001) 1113–1144.
[4] M. Newman, G. Barkema, Monte Carlo methods in statistical physics, Clarendon Press, Oxford, 1999.
[5] O. Penrose, Statistical mechanics and the kinetics of phase separation, in: J. Ball (Ed.), Material Instabilities in Continuum Mechanics and Related Mathematical Problems, Clarendon Press, Oxford, 1988, pp. 373–394.
[6] P. Voorhees, The theory of Ostwald ripening, J. Stat. Phys. 38 (1985) 231–252.
[7] P. Voorhees, Ostwald ripening in two-phase mixtures, Annu. Rev. Mater. Sci. 22 (1992) 197–215.
[8] J. Yao, K. Elder, H. Guo, M. Grant, Late stage droplet growth, Physica A 204 (1994) 770–788.
[9] P. Voorhees, R. Schaefer, In situ observation of particle motion and diffusion interactions during coarsening, Acta Metall. 35 (1987) 327–339.
[10] B. Niethammer, R. Pego, Non-self-similar behavior in the LSW theory of Ostwald ripening, J. Stat. Phys. 95 (1999) 867–902.
[11] G. McFadden, P. Voorhees, R. Boisvert, D. Meiron, A boundary integral method for the simulation of two-dimensional particle coarsening, J. Sci. Comput. 1 (1986) 117–144.
[12] P. Voorhees, G. McFadden, R. Boisvert, D. Meiron, Numerical simulation of morphological development during Ostwald ripening, Acta Metall. 36 (1988) 207–222.
[13] N. Akaiwa, D. Meiron, Two-dimensional late-stage coarsening for nucleation and growth at high-area fractions, Phys. Rev. E 54 (1996) R13–R16.
[14] T. Imaeda, K. Kawasaki, Theory of morphological evolution in Ostwald ripening, Physica A 186 (1992) 359–387.
[15] T. Hou, J. Lowengrub, M. Shelley, Boundary integral methods for multicomponent fluids and multiphase materials, J. Comput. Phys. 169 (2001) 302–362.
[16] F. Filbet, P. Laurençot, Numerical approximation of the Lifshitz–Slyozov–Wagner equation, SIAM J. Num. Anal. 41 (2003) 563–588.
[17] J. Carrillo, T. Goudon, A numerical study on large-time asymptotics of the Lifschitz–Slyozov system, J. Sci. Comput. 20 (2004) 69–113.
[18] C. Elliott, D. French, A non-conforming finite element method for the two-dimensional Cahn–Hilliard equation, SIAM J. Num. Anal. 26 (1989) 884–903.
[19] C. Elliott, D. French, Numerical studies of the Cahn–Hilliard equation for phase separation, IMA J. Appl. Math. 38 (1987) 97–128.
[20] J. Barrett, J. Blowey, Finite element approximation of the Cahn–Hilliard equation with concentration dependent mobility, Math. Comput. 68 (1999) 487–517.
[21] A. Chakrabarti, R. Toral, J. Gunton, Late-stage coarsening for off-critical quenches: scaling functions and the growth law, Phys. Rev. E 47 (1993) 3025–3038.
[22] J. Gunton, R. Toral, A. Chakrabarti, Numerical studies of phase separation in models of binary alloys and polymer blends, Physica Scripta T33 (1990) 12–19.
[23] T. Rogers, K. Elder, R. Desai, Numerical study of the late stages of spinodal decomposition, Phys. Rev. B 37 (1988) 9638–9649.
[24] T. Rogers, R. Desai, Numerical study of late-stage coarsening for off-critical quenches in the Cahn–Hilliard equation of phase separation, Phys. Rev. B 39 (1989) 11956–11964.
[25] E. de Mello, O. Filho, Numerical study of the Cahn–Hilliard equation in one, two, and three dimensions, Physica A 347 (2005) 429–443.
[26] K. Kawasaki, Diffusion constants near the critical point for time-dependent Ising models, Phys. Rev. 145 (1965) 224–230.
[27] J. Gunton, E. Gawlinski, K. Kaski, Numerical simulation studies of the kinetics of first-order phase transitions, in: S. Komura, H. Furukawa (Eds.), Dynamics of ordering processes in condensed matter, Plenum, New York, 1988, pp. 101–110.
[28] D. Landau, K. Binder, A guide to Monte Carlo simulations in statistical physics, Cambridge University Press, Cambridge, 2000.
[29] B. Zheng, Monte Carlo simulations of short-time critical dynamics, Int. J. Mod. Phys. B 12 (1998) 1419–1484.
[30] M. Katsoulakis, D. Vlachos, Coarse-grained stochastic processes and kinetic Monte Carlo simulators for the diffusion of interacting particles, J. Chem. Phys. 119 (2003) 9412–9427.
[31] M. Katsoulakis, A. Majda, D. Vlachos, Coarse-grained stochastic processes and Monte Carlo simulations in lattice systems, J. Comput. Phys. 186 (2003) 250–278.

[32] M. Katsoulakis, A. Majda, D. Vlachos, Coarse-grained stochastic processes for microscopic lattice systems, Proc. Natl. Acad. Sci. 100 (2003) 782–787.
[33] J. Lebowitz, E. Orlandi, E. Presutti, A particle model for spinodal decomposition, J. Stat. Phys. 63 (1991) 933–974.
[34] M. Katsoulakis, P. Souganidis, Stochastic Ising models and anisotropic front propagation, J. Stat. Phys. 87 (1997) 63–90.
[35] M. Hildebrand, A.S. Mikhailov, Mesoscopic modeling in the kinetic theory of adsorbates, J. Phys. Chem. 100 (1996) 19089–19101.
[36] G. Giacomin, J. Lebowitz, Exact macroscopic description of phase segregation in model alloys with long range interactions, Phys. Rev. Lett. 76 (1996) 1094–1097.
[37] D. Horntrop, M. Katsoulakis, D. Vlachos, Spectral methods for mesoscopic models of pattern formation, J. Comput. Phys. 173 (2001) 364–390.
[38] J. Gaines, Numerical experiments with S(P)DE's, in: A. Etheridge (Ed.), Stochastic Partial Differential Equations, Cambridge University Press, Cambridge, 1995, pp. 55–71.
[39] I. Gyöngy, Approximations of stochastic partial differential equations, in: G. Da Prato, L. Tubaro (Eds.), Stochastic Partial Differential Equations and Applications, Marcel Dekker, New York, 2002, pp. 287–307.
[40] I. Gyöngy, Lattice approximations for stochastic quasi-linear parabolic partial differential equations driven by space-time white noise I, Potential Anal. 9 (1998) 1–25.
[41] I. Gyöngy, Lattice approximations for stochastic quasi-linear parabolic partial differential equations driven by space-time white noise, Potential Anal. 11 (1999) 1–37.
[42] I. Gyöngy, N. Krylov, On the splitting-up method and stochastic partial differential equations, Ann. Prob. 31 (2003) 564–591.
[43] M. Seesselberg, F. Petruccione, Numerical integration of stochastic partial differential equations, Comput. Phys. Commun. 74 (1993) 303–315.
[44] H. Yoo, Semi-discretization of stochastic partial differential equations on R1, Math. Comput. 69 (2000) 653–666.
[45] R. Ghanem, P. Spanos, Stochastic finite elements: a spectral approach, Springer, New York, 1991.
[46] E. Allen, S. Novosel, Z. Zheng, Finite element and difference approximation of some linear stochastic partial differential equations, Stochast. Stochast. Rep. 64 (1998) 117–142.
[47] M. Deb, I. Babuška, J. Oden, Solution of stochastic partial differential equations using Galerkin finite element techniques, Comput. Met. Appl. Mech. Eng. 190 (2001) 6359–6372.
[48] Q. Du, T. Zhang, Numerical approximation of some linear stochastic partial differential equations driven by special additive noises, SIAM J. Num. Anal. 40 (2002) 1421–1445.
[49] L. Machiels, M. Deville, Numerical simulation of randomly forced turbulent flows, J. Comput. Phys. 145 (1998) 246–279.
[50] D. Horntrop, Spectral schemes for stochastic partial differential equations, submitted.
[51] C. Canuto, M. Hussaini, A. Quarteroni, T. Zang, Spectral methods in fluid dynamics, Springer, New York, 1988.
[52] D. Vlachos, M. Katsoulakis, Derivation and validation of mesoscopic theories for diffusion-reaction of interacting molecules, Phys. Rev. Lett. 85 (2000) 3898–3901.
[53] R. Lam, T. Basak, D. Vlachos, M. Katsoulakis, Validation of mesoscopic theories and their application to computing concentration dependent diffusivities, J. Chem. Phys. 115 (2001) 11278–11288.
[54] J. Doob, Stochastic processes, Wiley, New York, 1953.
[55] F. Elliott, A. Majda, D. Horntrop, R. McLaughlin, Hierarchical Monte Carlo methods for fractal random fields, J. Stat. Phys. 81 (1995) 717–736.
[56] F. Elliott, D. Horntrop, A. Majda, Monte Carlo methods for turbulent tracers with long range and fractal random velocity fields, Chaos 7 (1997) 39–48.
[57] F. Elliott, D. Horntrop, A. Majda, A Fourier-wavelet Monte Carlo method for fractal random fields, J. Comput. Phys. 132 (1997) 384–408.
[58] D. Horntrop, A. Majda, An overview of Monte Carlo simulation techniques for the generation of random fields, in: P. Muller, D. Henderson (Eds.), Monte Carlo simulations in oceanography, Proceedings of the Ninth Aha Huliko Hawaiian Winter Workshop, 1997, pp. 67–79.
[59] S. Prigarin, Spectral models of random fields in Monte Carlo methods, VSP, Utrecht, 2001.
[60] K. Sabelfeld, Monte Carlo methods, Springer, Berlin, 1991.
[61] P. Kramer, O. Kurbanmuradov, K. Sabelfeld, Extensions of multiscale Gaussian random field simulation algorithms, submitted.
[62] P. Kloeden, E. Platen, Numerical solution of stochastic differential equations, Springer, Berlin, 1992.
[63] K. Burrage, E. Platen, Runge–Kutta methods for stochastic differential equations, Ann. Num. Math. 1 (1994) 63–78.
[64] K. Burrage, P. Burrage, High strong order explicit Runge–Kutta methods for stochastic ordinary differential equations, Appl. Num. Math. 22 (1996) 81–101.
[65] S. Glotzer, E. Di Marzio, M. Muthukumar, Reaction-controlled morphology of phase-separating mixtures, Phys. Rev. Lett. 74 (1995) 2034–2037.
[66] V. Fradkov, M. Glicksman, S. Marsh, Coarsening kinetics in finite clusters, Phys. Rev. E 53 (1996) 3925–3932.
[67] A. Hönig, B. Niethammer, F. Otto, On first-order corrections to the LSW theory I: infinite systems, J. Stat. Phys. 119 (2005) 61–122.
[68] A. Hönig, B. Niethammer, F. Otto, On first-order corrections to the LSW theory II: finite systems, J. Stat. Phys. 119 (2005) 123–164.
[69] H. Mandyam, M. Glicksman, J. Helsing, S. Marsh, Statistical simulations of diffusional coarsening in finite clusters, Phys. Rev. E 58 (1998) 2119–2130.
[70] D. Horntrop, Mesoscopic simulation for self-orgranization in surface processes, in: V. Sunderam, et al. (Eds.), Computational Science-ICCS 2005, Springer Lecture Notes in Computer Science, vol. 3514, 2005, pp. 852–859.